

Kinetic-Ballooning-Bifurcation in Tokamak Pedestals Across Shaping and Aspect-Ratio

J. F. Parisi^{1,*}, A. O. Nelson², R. Gaur³, S. M. Kaye¹, F. I. Parra¹, J. W. Berkery¹, K. Barada⁴, C. Clauser⁵, A. J. Creely⁶, A. Diallo¹, W. Guttenfelder^{1,7}, J. W. Hughes⁵, L. A. Kogan⁸, A. Kleiner¹, A. Q. Kuang⁶, M. Lampert¹, T. Macwan⁴, J. E. Menard¹, and M. A. Miller⁵

¹Princeton Plasma Physics Laboratory, Princeton University, Princeton, NJ, USA

²Department of Applied Physics and Applied Mathematics, Columbia University, New York, NY, USA

³Department of Mechanical and Aerospace Engineering, Princeton University, Princeton, NJ, USA

⁴University of California, Los Angeles, Los Angeles, CA, USA

⁵Plasma Science and Fusion Center, Massachusetts Institute of Technology, Cambridge, MA, USA

⁶Commonwealth Fusion Systems, Cambridge, MA, USA

⁷Type One Energy, 8383 Greenway Boulevard, Middleton, WI, USA and

⁸United Kingdom Atomic Energy Authority, Culham Science Centre, Abingdon, UK

We employ a new gyrokinetic threshold model to predict a bifurcation in tokamak pedestal width and height scalings that depends strongly on plasma shaping and aspect-ratio. This bifurcation arises from the first and second stability properties of kinetic-ballooning-modes that yield wide and narrow pedestal branches, opening up the operating space of accessible pedestal widths and heights. The wide branch offers potential for edge-localized-mode-free pedestals with a high core pressure. For negative triangularity, low-aspect-ratio configurations are predicted to give steeper pedestals than conventional-aspect-ratio. Both wide and narrow branches have been attained in tokamak experiments.

Introduction. – The realization of magnetic confinement fusion energy represents a significant milestone in the quest for clean and abundant power sources. This endeavor hinges on the ability to confine a high-pressure plasma within a magnetic field, as characterized by the ratio β ($\beta = 2\mu_0 p/B^2$ where p is the plasma pressure and B is the magnetic field strength). For tokamaks operating in high-confinement mode (H-mode), an intriguing phenomenon emerges—the formation of a pedestal at the plasma edge [1], often enhancing β substantially and hence fusion power. However, ballooning modes pose a fundamental challenge to achieving optimal β values. Recent experiments in negative triangularity plasmas [2, 3] showed that plasma shaping changes pedestal ballooning stability substantially. In this Letter, we describe a bifurcation in the H-mode pedestal width and height that can be manipulated and optimized with plasma shaping and aspect-ratio. The bifurcation arises from the dynamics of ballooning stability and offers the possibility of new pedestal operating scenarios for fusion reactors. By degrading ballooning stability in the edge, higher core β may be achieved by enabling the pedestal to grow without triggering edge-localized-modes (ELMs) that threaten plasma-facing components [4, 5].

Pedestal Prediction. – Predictive pedestal models posit that the pedestal’s radial width Δ_{ped} and normalized pressure height $\beta_{\theta,\text{ped}}$ are constrained by ballooning and ELM stability [5]. The microscopic ballooning constraint gives a width-height scaling that bounds the pedestal pressure gradients and the macroscopic ELM constraint gives a ‘hard’ limit that transports significant energy and particles once triggered [6, 7]. These two constraints intersect to give a Δ_{ped} , $\beta_{\theta,\text{ped}}$ prediction. Previous work

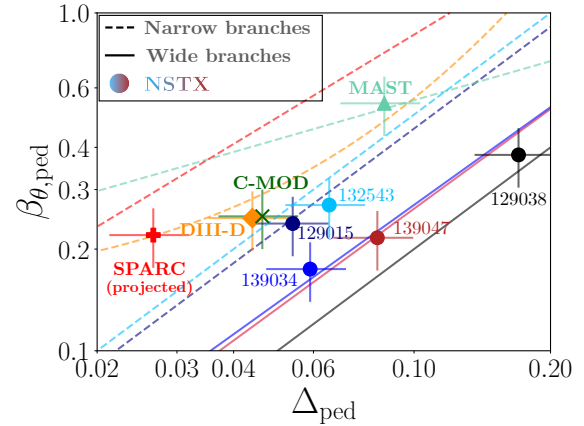


FIG. 1: Bifurcation of pedestal height $\beta_{\theta,\text{ped}}$ versus width Δ_{ped} for C-MOD, DIII-D, MAST, NSTX, and SPARC discharges, with width-height scalings of branch nearest to the equilibrium point (solid = wide branch, dashed = narrow branch). NSTX discharge numbers are indicated next to circle markers, DIII-D #163303, MAST #29782, C-MOD #1101214029.

has shown that the ELM constraint is sensitive to plasma shaping: negative triangularity TCX tokamak plasmas were subject to a much more restrictive ELM constraint than positive triangularity [8], whereas on the DIII-D tokamak, fueling and strong positive triangularity provided a route to ‘Super H-mode’ [9, 10] pedestal. The new bifurcation in this work is complementary to these results, focusing on kinetic-ballooning-mode physics.

Ballooning Bifurcation. – The kinetic-ballooning-mode (KBM) [11] has two stability branches. At relatively low normalized pressure gradients ($\alpha = -q^2 R_0 \nabla \beta \lesssim 1$), α increases until the destabilizing pressure gradients overcome the stabilizing effects of field-line

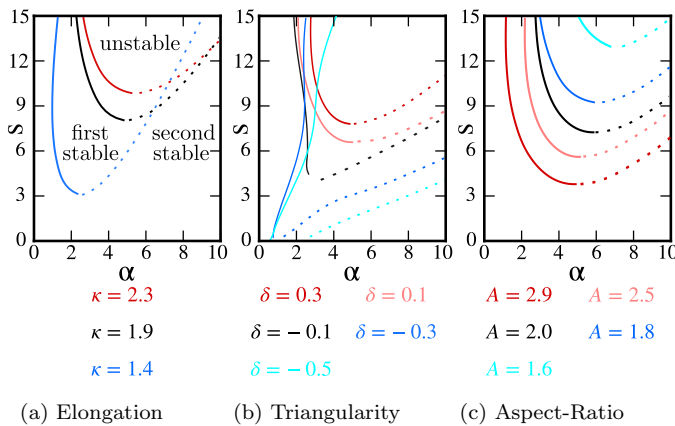


FIG. 2: Ideal $s - \alpha$ diagrams for different elongation, triangularity, and aspect-ratio at the nominal pedestal width and height at the mid-pedestal flux surface for NSTX 139047. First and second stability curves are solid and dashed, respectively. In (a), first-stable, second-stable, and unstable regions are indicated for $\kappa = 1.9$.

bending [12]. Here, q is the magnetic safety factor and R_0 is the magnetic axis major radius. At much higher α , the local magnetic shear at the low-field side becomes highly negative and stabilizing, which leads to second stability [13]. A key result of this work is that first and second KBM stability across the pedestal is realized as two distinct branches – wide and narrow – of ballooning width-height scalings.

In Figure 1, we show the pedestal width-height bifurcation for five National-Spherical-Torus-Experiment (NSTX) discharges 129015, 129038 [14], 132543, 139034, and 139047 [15]. To obtain the width-height scaling lines in Figure 1, a linear KBM threshold model [16] is used. The scaling indicates the boundary between accessible and inaccessible equilibria. Each NSTX discharge admitted two scaling solutions: a wide and narrow branch. However, 139034, 139047, and 129038 equilibria – indicated by markers in Figure 1 – lie on the wide branch, whereas 129015 and 132543 lie on the narrow branch. These five discharges demonstrate that NSTX experiments have occupied both wide and narrow pedestal branches. For readability, in Figure 1 we only plot the branch closest to the actual equilibrium. We also plot the equilibrium points and width-height scaling for DIII-D 163303 [17], which lies in the narrow branch, MAST 29782 [18], also on the narrow branch, and a projected full-field SPARC case [19–21], whose operational point is projected to be below the narrow branch. While we do not calculate a scaling, we show the C-MOD 1101214029 equilibrium point [22] lies in the narrow branch region.

Magnetic Shaping And Aspect-Ratio – We now demonstrate how plasma shaping and aspect-ratio enter the ballooning bifurcation. The geometric shape of the last-closed-flux-surface and its penetration to the magnetic axis has a large impact on plasma performance [2, 23–25] and is well-known to change ballooning mode sta-

bility [26, 27]. Starting from an experimental equilibrium for NSTX 139047, we vary the shaping parameters and aspect-ratio. We choose a Luce parameterization for the plasma shape [28], defining the flux surface elongation κ and triangularity δ as the average $\langle \dots \rangle_L$ of the Luce parameters $\kappa = \langle \kappa \rangle_L$, $\delta = \langle \delta \rangle_L$. When varying δ , the total plasma current I_p and normalized pressure $\beta_N = 2\mu_0 \langle p \rangle a / I_p B_{T0}$ are kept constant. Here, $\langle p \rangle$ is the volume-averaged pressure, a is the minor radius, and B_{T0} is the toroidal magnetic field strength at the magnetic axis. When varying κ , we scale the plasma current as $I_p \sim 1 + \kappa^2$, and when varying aspect-ratio $A = R_0/a$, we scale $\beta_N \sim 1/\sqrt{R_0}$, $B_{T0} \sim R_0$, $I_p \sim \sqrt{R_0}$.

First, we describe the effect of shaping and aspect-ratio on ideal MHD ballooning stability to understand how shaping and aspect-ratio enter the width-height scaling. For NSTX 139047, we compare equilibria with different elongation, triangularity, and aspect-ratio by performing $s - \alpha$ analysis [13] for ideal-ballooning-modes (IBMs) on the mid-pedestal flux surface, plotting stability versus magnetic shear $s = (r/q)(dq/dr)$ and α where r is the flux-surface half-diameter. In Figure 2 (a), increasing elongation from $\kappa = 1.4$ to 2.3 shifts the first-stable boundary to much higher s and α . This suggests that a first-stable branch will be much wider at lower elongation because the first-stable boundary is at lower α values. Similarly in Figure 2 (b), decreasing triangularity to negative values decreases the s and α values for the first-stable boundary, suggesting that a first-stable branch will be much wider at lower and negative triangularity. Finally, Figure 2 (c) suggests that the first-stable branch will be widest at high-aspect-ratio.

In Figure 3(a) and (b), the above predictions are borne out with width-height scaling results using the KBM and the IBM for a triangularity scan. We emphasize that we have performed self-consistent equilibrium variation along with stability analysis, as outlined in [16]. As predicted from $s - \alpha$ analysis in Figure 2, the wide branch in Figure 3(a) widens with larger negative triangularity, whereas for the narrow branch, larger positive triangularity increases the width. The wide and narrow branches scalings for the KBM are

$$\Delta_{\text{ped,wide}} \sim 0.5^\delta, \quad \Delta_{\text{ped,narrow}} \sim 1.7^\delta. \quad (1)$$

Shown in Figure 3(b) for the IBM, while the trends for Δ_{ped} are similar as for the KBM in Figure 3(a), for $\delta \gtrsim -0.1$, the wide branch ceases to exist for the IBM, with only the narrow branch remaining. It is well-documented that the first and second stability boundaries can differ significantly between ideal and kinetic-ballooning-modes [11, 16, 29–33]. For the example in Figure 3, in first-stability the critical KBM α is smaller in value, but in second-stability the critical KBM α tends to be larger. Above certain triangularity values, in this example $\delta \gtrsim -0.1$, pedestal equilibria can no longer access first-stability for the IBM. Such a difference in the

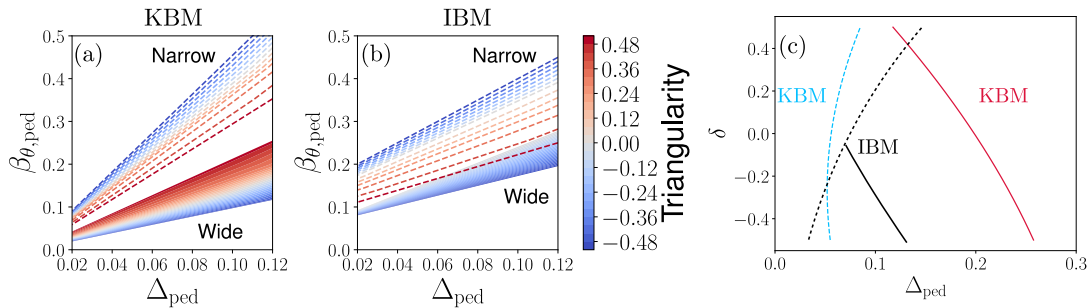


FIG. 3: Width-height scalings across triangularity using (a) the kinetic-ballooning-mode (KBM) and (b) the ideal-ballooning-mode (IBM). In (c), we take a constant $\beta_{\theta,\text{ped}} = 0.25$ slice and plot the triangularity δ versus pedestal width Δ_{ped} . A bifurcation exists for all values of δ in the KBM scalings, but not for the IBM scalings.

width-height scaling between the ideal and kinetic calculation of ballooning modes is important because previous treatment of the width-height scaling uses the ideal ballooning mode [5, 34], and hence, bifurcations may not always be predicted with an ideal MHD treatment.

We now show the effect of elongation and aspect-ratio on width-height scalings. In Figure 4, the left column shows the width at constant $\beta_{\theta,\text{ped}} = 0.25$, with the elongation and aspect-ratio dependence of the width scaling for the wide and narrow branches,

$$\begin{aligned} \Delta_{\text{ped,wide}} &\sim A^{1.5}, \quad \Delta_{\text{ped,wide}} \sim \kappa^{-1.8} \\ \Delta_{\text{ped,narrow}} &\sim A^{-0.9}, \quad \Delta_{\text{ped,narrow}} \sim \kappa^{2.9}. \end{aligned} \quad (2)$$

In the right column of Figure 4, we show the scalings for a range of $\beta_{\theta,\text{ped}}$ values. Curiously, at conventional-aspect-ratio $\gtrsim 2.5$, the wide branch has such gentle gradients

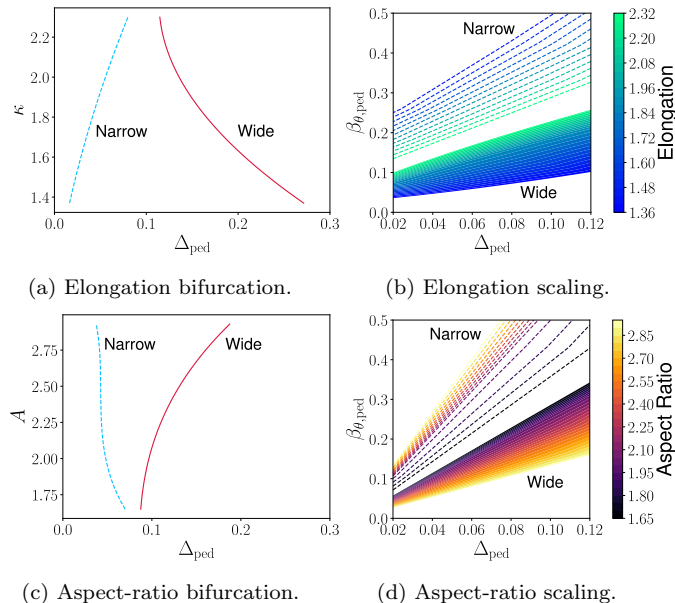


FIG. 4: Left column: first and second-stable kinetic-ballooning-mode prediction for pedestal width at $\beta_{\theta,\text{ped}} = 0.25$ for elongation and aspect-ratio. Right column: corresponding width-height scaling expressions.

that they are closer to L-mode-like values ($-a\nabla\ln(T_e) \ll 10$), which might explain why no conventional-aspect-ratio H-mode experiments we have studied were in the wide-branch, despite finding wide-branch solutions in such equilibria. Notably, elongated, low-aspect-ratio plasmas, such as in NSTX, have a smaller gap in $\Delta_{\theta,\text{ped}}$ between the narrow and wide branches, which might explain why the first and second branches are accessible for NSTX, shown in Figure 1.

The strong dependence of the width-height scalings on shaping and aspect-ratio can be understood by the effect of these parameters on the magnetic geometry. In Figure 5, we plot the local magnetic shear [13],

$$s_{\text{local}} = -\mathbf{B} \cdot \nabla \left(\frac{\nabla\Lambda \cdot \nabla\psi}{|\nabla\psi|^2} \right), \quad (3)$$

for the mid-pedestal flux surface, which measures the change of the safety factor in the parallel direction along a flux surface. Here, ψ is the poloidal flux and Λ is a magnetic field-line label for a magnetic field $\mathbf{B} = \nabla\psi \times \nabla\Lambda$. In Figure 5, we also plot the in-flux-surface magnetic curvature drift frequency,

$$\omega_{\kappa} = G \frac{\partial\psi}{\partial r} \left[\left(\frac{\mathbf{B}}{B} \times \nabla(B + \beta) \right) \cdot \nabla\Lambda \right], \quad (4)$$

for a range of elongation, triangularity, and aspect-ratio equilibria with the same pedestal width and height. The dimensionless quantity ω_{κ} is normalized to the ion parallel streaming frequency using the quantity G . For ballooning modes, weaker magnetic shear and faster magnetic drifts tend to stabilize the modes. Crucially, the local shear stabilization is sign-independent [13]. Because ballooning eigenmodes peak in magnitude close to the low-field-side with poloidal angle $\theta \approx 0$, the values of s_{local} and ω_{κ} around $\theta \approx 0$ most strongly determine ballooning mode stability. Figure 5 shows that lower values of elongation, more negative triangularity, and higher aspect-ratio decrease the local shear and increase ω_{κ} , all of which destabilize the KBM. This is consistent with Figure 2 where, for example, in Figure 2(a), relatively

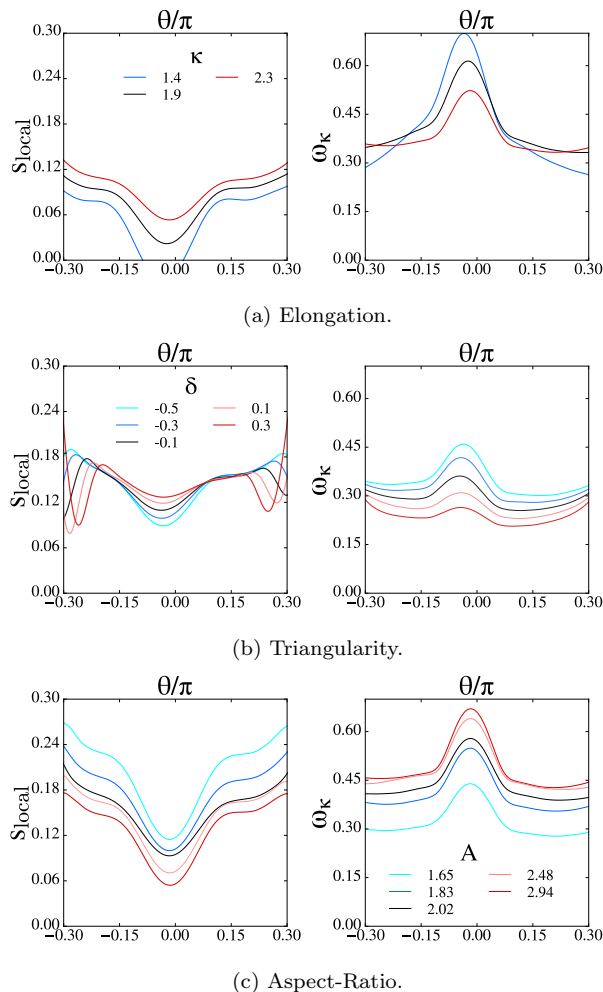


FIG. 5: Local magnetic shear (left column) and magnetic curvature drift frequency (right column) versus poloidal angle on the mid-pedestal flux surface for (a) elongation, (b) triangularity, and (c) aspect-ratio scans. Quantities s_{local} and ω_{κ} are defined in Equations (3) and (4).

small values of α are needed to destabilize the ballooning mode at lower elongation, which has relatively small s_{local} around $\theta = 0$ and very fast magnetic drifts. The impact of the variation of kinetic effects such as drift resonances and Landau damping across shaping and aspect-ratio, while included in our gyrokinetic simulations, has not been studied here. Determining their importance is an important question for future work.

We have discovered that the width-height scaling (a) has a bifurcation, and (b) has a strong dependence on shaping and aspect-ratio. We now employ these findings to predict favorable ELM-free regimes.

ELM-Free Operation. – It has been suggested that degraded pedestal gradients might permit ELM-free operation while achieving a high pedestal pressure [4]. Such robust ELM-free operation could be achieved by operating in the wide KBM branch. In Figure 6, we schematically show the wide and narrow KBM branches, with color contours heuristically representing different shaping and

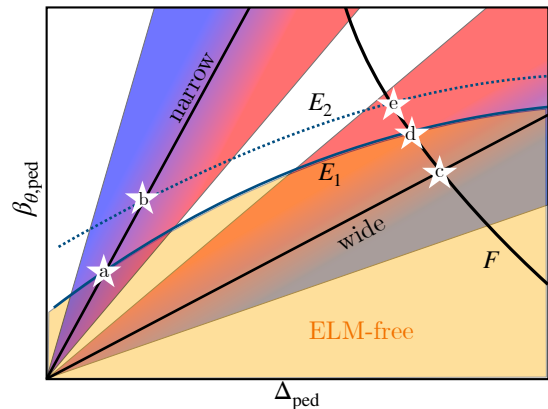


FIG. 6: Schematic dependence of pedestal equilibrium points (stars) on wide and narrow KBM branches, first and second ELM stability (E_1 , E_2), and an alternative saturation mechanism such as flow shear (F). The color contours represent different shaping and aspect-ratio configurations.

aspect-ratio configurations based on results in Figures 3 and 4. Figure 6 presents several possible equilibrium points; Point (a): a conventional-aspect-ratio ELMy H-mode pedestal typically saturates where first ELM stability, curve E_1 , intersects the narrow branch at the star marker (a). We have assumed that the ELM constraint has the scaling dependence $\Delta_{\text{ped}} \sim \beta_{\theta, \text{ped}}^{4/3}$ [35]. Point (b): Super H-modes [10] are obtained by accessing second ELM stability E_2 , which results in a pedestal at point (b). While (b) achieved a much higher pedestal height, it may still suffer from ELMs.

It may be possible to move to a much higher $\beta_{\theta, \text{ped}}$ value and avoid ELMs by accessing the wide pedestal branch. In Figure 6 we have added a new constraint F that could be due to additional transport, $\mathbf{E} \times \mathbf{B}$ flow shear, or other saturation mechanisms; the dependence of F on Δ_{ped} and $\beta_{\theta, \text{ped}}$ will depend on the saturation mechanism, but our preliminary analysis shows that $\Delta_{\text{ped}} \sim \beta_{\theta, \text{ped}}^{-1}$ for a $\mathbf{E} \times \mathbf{B}$ flow shear constraint. The intersection of the wide branch and F could result in a much higher and wider ELM-free pedestal at point (c). However ELMy solutions may still exist on the wide branch: if an even higher $\beta_{\theta, \text{ped}}$ is desired, shaping and aspect-ratio could be adjusted to move to points (d) or (e), which are intersections of the wide branch and first and second ELM stability. For this illustration, we have omitted details of how plasma shaping and aspect-ratio changes ELM stability [8, 9]. Systematically determining the dependencies of *both* the ELM and KBM scalings on shaping and aspect-ratio is an important problem.

Low-Aspect-Ratio Negative Triangularity H-Modes. – At low-aspect-ratio, negative triangularity (NT) might be particularly attractive for ELM-free H-mode operation. NT configurations [2] have recently received increased attention due to their ELM-free [3] and enhanced confinement characteristics [36]. By design, such NT configurations do not access H-mode, staying in first ballooning stability intentionally [27] because accessing H-mode

would likely entail an undesirable ELM, corresponding to point (a) or (b) in Figure 6. While NT at conventional aspect-ratio can degrade first-stable pedestals so much that the edge gradients are L-mode-like, at *low-aspect-ratio* NT could achieve steeper gradients. This is because Figure 4(c) shows the wide branch has roughly twice as steep gradients at $A = 1.7$ compared with $A = 2.8$ due to $\Delta_{\text{ped,wide}} \sim A^{1.5}$ (see Equation (2)). Thus, a low-aspect-ratio NT H-mode might inherit the favorable properties of negative triangularity (no narrow branch access), while being able to access H-mode-like gradients.

Branch-Jumping. – Finally, we note a curious consequence of the width-height bifurcation: a sufficiently big and sudden loss (or gain) of pedestal particles and heat – such as an ELM (or pellet injection) – could cause a pedestal to jump from the narrow to wide branch (or wide to narrow branch) in Figure 6. There are examples of H-modes that become ELM-free after an initial ELM [37]; jumping from narrow to wide branches is a possible explanation for these observations. Finally, two companion NSTX discharges shown in Figure 1, 129015 and 129038 [14], fall in the the narrow and wide branches. These discharges differ mainly by the amount of Lithium dosing, which might ultimately be responsible for different branch access.

Summary. – We have discovered a novel and intriguing bifurcation in the width-height scalings of tokamak pedestals, which can be significantly modified by plasma shaping and aspect-ratio. This bifurcation arises from the interplay between first and second stability properties of kinetic-ballooning-modes and allows for the existence of both wide and narrow pedestal branches. Importantly, this discovery opens up the operating space for accessible pedestal widths and heights, offering new prospects for pedestal control in current and future fusion experiments. While our investigations thus far have only revealed wide branch access in NSTX pedestals, investigation of how NSTX pedestals accessed the wide branch could provide a pathway to ELM-free operation while achieving high pedestal pressures.

Acknowledgements. – We are grateful to S. C. Cowley, W. Dorland, R. Maingi, O. Sauter, P. B. Snyder, and H. R. Wilson for insightful discussions. This work was supported by the U.S. Department of Energy under contract numbers DE-AC02-09CH11466, DE-SC0022270, DE-SC0022272, and the Department of Energy Early Career Research Program. The United States Government retains a non-exclusive, paid-up, irrevocable, world-wide license to publish or reproduce the published form of this manuscript, or allow others to do so, for United States Government purposes.

* jparisi@pppl.gov

- [1] F. Wagner, G. Becker, K. Behringer, D. Campbell, A. Eberhagen, W. Engelhardt, G. Fussmann, O. Gehre, J. Gernhardt, G. v. Gierke, G. Haas, M. Huang, F. Karger, M. Keilhacker, O. Klüber, M. Kornherr, K. Lackner, G. Lisitano, G. G. Lister, H. M. Mayer, D. Meisel, E. R. Müller, H. Murmann, H. Niedermeyer, W. Poschenrieder, H. Rapp, H. Röhr, F. Schneider, G. Siller, E. Speth, A. Stäbler, K. H. Steuer, G. Venus, O. Vollmer, and Z. Yü, *Physical Review Letters* **49**, 1408 (1982).
- [2] M. E. Austin, A. Marinoni, M. L. Walker, M. W. Brookman, J. S. Degraessie, A. W. Hyatt, G. R. McKee, C. C. Petty, T. L. Rhodes, S. P. Smith, C. Sung, K. E. Thome, and A. D. Turnbull, *Physical Review Letters* **122**, 115001 (2019).
- [3] A. Nelson, L. Schmitz, C. Paz-Soldan, K. E. Thome, T. B. Cote, N. Leuthold, F. Scotti, M. E. Austin, A. Hyatt, and T. Osborne, *Physical Review Letters* (2023).
- [4] T. H. Osborne, G. L. Jackson, Z. Yan, R. Maingi, D. K. Mansfield, B. A. Grierson, C. P. Chrobak, A. G. McLean, S. L. Allen, D. J. Battaglia, A. R. Briesemeister, M. E. Fenstermacher, G. R. McKee, and P. B. Snyder, *Nuclear Fusion* **55** (2015).
- [5] P. B. Snyder, N. Aiba, M. Beurskens, R. J. Groebner, L. D. Horton, A. E. Hubbard, J. W. Hughes, G. T. Huysmans, Y. Kamada, A. Kirk, C. Konz, A. W. Leonard, J. Lönroth, C. F. Maggi, R. Maingi, T. H. Osborne, N. Oyama, A. Pankin, S. Saarelma, G. Saibene, J. L. Terry, H. Urano, and H. R. Wilson, *Nuclear Fusion* **49**, 085035 (2009).
- [6] P. B. Snyder, H. R. Wilson, J. R. Ferron, L. L. Lao, A. W. Leonard, T. H. Osborne, A. D. Turnbull, D. Mossessian, M. Murakami, and X. Q. Xu, *Physics of Plasmas* **9**, 2037 (2002).
- [7] H. R. Wilson and S. C. Cowley, *Physical Review Letters* **92** (2004).
- [8] A. Merle, O. Sauter, and S. Y. Medvedev, *Plasma Physics and Controlled Fusion* **59**, 104001 (2017).
- [9] P. B. Snyder, W. M. Solomon, K. H. Burrell, A. M. Garofalo, B. A. Grierson, R. J. Groebner, A. W. Leonard, R. Nazikian, T. H. Osborne, E. A. Belli, J. Candy, and H. R. Wilson, *Nuclear Fusion* **55** (2015).
- [10] P. B. Snyder, J. W. Hughes, T. H. Osborne, C. Paz-Soldan, W. M. Solomon, M. Knolker, D. Eldon, T. Evans, T. Golfopoulos, B. A. Grierson, R. J. Groebner, A. E. Hubbard, E. Kolemen, B. Labombard, F. M. Laggner, O. Meneghini, S. Mordijck, T. Petrie, S. Scott, H. Q. Wang, H. R. Wilson, and Y. B. Zhu, *Nuclear Fusion* **59**, 086017 (2019).
- [11] W. M. Tang, J. W. Connor, and R. J. Hastie, *Nuclear Fusion* **20**, 1439 (1980).
- [12] J. W. Connor, R. J. Hastie, and J. B. Taylor, *Proc R Soc London Ser A* **365**, 3651 (1979).
- [13] J. M. Greene and M. S. Chance, *Nuclear Fusion* (1981).
- [14] R. Maingi, D. Boyle, J. Canik, S. Kaye, C. Skinner, J. Alain, M. Bell, R. Bell, S. Gerhardt, T. Gray, M. Jaworski, R. Kaita, H. Kugel, B. LeBlanc, J. Manickam, D. Mansfield, J. Menard, T. Osborne, R. Raman, A. Roquemore, S. Sabbagh, P. Snyder, and V. Soukhanovskii, *Nuclear Fusion* **52**, 083001 (2012).
- [15] A. Diallo, J. Canik, T. Göerler, S. H. Ku, G. J. Kramer, T. Osborne, P. Snyder, D. R. Smith, W. Guttenfelder, R. E. Bell, D. P. Boyle, C. S. Chang, B. P. Leblanc, R. Maingi, M. Podestà, and S. Sabbagh, *Nuclear Fusion*

- 53**, 093026 (2013).
- [16] J. F. Parisi, W. Guttenfelder, A. O. Nelson, R. Gaur, A. Kleiner, M. Lampert, G. Avdeeva, J. W. Berkery, C. Clauser, M. Curie, A. D'Allo, W. Dorland, and J. McClenaghan, "Kinetic-ballooning-limited pedestals in spherical tokamak plasmas (<https://arxiv.org/abs/2308.05238>)," (2023).
- [17] B. A. Grierson, X. Yuan, M. Gorelenkova, S. Kaye, N. C. Logan, O. Meneghini, S. R. Haskey, J. Buchanan, M. Fitzgerald, S. P. Smith, L. Cui, R. V. Budny, and F. M. Poli, **74**, 101 (2018).
- [18] S. F. Smith, A. Kirk, B. Chapman-Opoloioiu, J. G. Clark, C. J. Ham, L. Horvath, C. F. Maggi, R. Scannell, and S. Saarelma, *Plasma Physics and Controlled Fusion* **64** (2022).
- [19] A. J. Creely, M. J. Greenwald, S. B. Ballinger, D. Brunner, J. Canik, J. Doody, T. Fülöp, D. T. Garnier, R. Granetz, T. K. Gray, C. Holland, N. T. Howard, J. W. Hughes, J. H. Irby, V. A. Izzo, G. J. Kramer, A. Q. Kuang, B. LaBombard, Y. Lin, B. Lipschultz, N. C. Logan, J. D. Lore, E. S. Marmor, K. Montes, R. T. Mungaard, C. Paz-Soldan, C. Rea, M. L. Reinke, P. Rodriguez-Fernandez, K. Särkimäki, F. Sciortino, S. D. Scott, A. Snicker, P. B. Snyder, B. N. Sorbom, R. Sweeney, R. A. Tinguely, E. A. Tolman, M. Uman-sky, O. Vallhagen, J. Varje, D. G. Whyte, J. C. Wright, S. J. Wukitch, and J. Zhu, *Journal of Plasma Physics* **86** (2020).
- [20] J. W. Hughes, N. T. Howard, P. Rodriguez-Fernandez, A. J. Creely, A. Q. Kuang, P. B. Snyder, T. M. Wilks, R. Sweeney, and M. Greenwald, *Journal of Plasma Physics* (2020).
- [21] A. Q. Kuang, T. Looby, J. Pavone, and A. Creely, "Sparcpublic," <https://github.com/cfs-energy/SPARCPublic> (2022).
- [22] J. Hughes, P. Snyder, J. Walk, E. Davis, A. D'Allo, B. LaBombard, S. Baek, R. Churchill, M. Greenwald, R. Groebner, A. Hubbard, B. Lipschultz, E. Marmor, T. Osborne, M. Reinke, J. Rice, C. Theiler, J. Terry, A. White, D. Whyte, S. Wolfe, and X. Xu, *Nuclear Fusion* **53**, 043016 (2013).
- [23] R. J. Goldston, *Plasma Physics and Controlled Fusion* **26**, 87 (1984).
- [24] S. Kaye and R. Goldston, *Nuclear Fusion* **25**, 65 (1985).
- [25] J. Ball and F. I. Parra, *Plasma Physics and Controlled Fusion* **57**, 035006 (2015).
- [26] A. D. Turnbull, Y. R. Lin-Liu, R. L. Miller, T. S. Taylor, and T. N. Todd, *Physics of Plasmas* **6**, 1113 (1999).
- [27] A. Nelson, C. Paz-Soldan, and S. Saarelma, *Nuclear Fusion* **62**, 096020 (2022).
- [28] T. C. Luce, *Plasma Physics and Controlled Fusion* **55**, 095009 (2013).
- [29] R. J. Hastie and K. W. Hesketh, *Nuclear Fusion* **21** (1981).
- [30] J. Dong, L. Chen, and F. Zonca, *Nuclear Fusion* **39** (1999).
- [31] M. J. Pueschel, M. Kammerer, and F. Jenko, *Physics of Plasmas* **15** (2008).
- [32] C. H. Ma and X. Q. Xu, *Nuclear Fusion* **57** (2017).
- [33] K. Aleynikova and A. Zocco, *Physics of Plasmas* **24** (2017).
- [34] S. Saarelma, C. D. Challis, L. Garzotti, L. Frassinetti, C. F. Maggi, M. Romanelli, C. Stokes, and J. Contributors, *Plasma Physics and Controlled Fusion* **60** (2017).
- [35] P. B. Snyder, R. J. Groebner, J. W. Hughes, T. H. Osborne, M. Beurskens, A. W. Leonard, H. R. Wilson, and X. Q. Xu, *Nuclear Fusion* **51**, 103016 (2011).
- [36] C. Paz-Soldan, C. Chrystal, P. Lunia, A. O. Nelson, K. E. Thome, M. E. Austin, T. B. Cote, A. W. Hyatt, A. Marinoni, T. H. Osborne, M. Pharr, O. Sauter, F. Scotti, T. M. Wilks, and H. S. Wilson, "Simultaneous access to high normalized current, pressure, density, and confinement in strongly-shaped diverted negative triangularity plasmas," (2023), arXiv:2309.03689.
- [37] R. Maingi, R. E. Bell, J. M. Canik, S. P. Gerhardt, S. M. Kaye, B. P. LeBlanc, T. H. Osborne, M. G. Bell, E. D. Fredrickson, K. C. Lee, J. E. Menard, J.-K. Park, S. A. Sabbagh, and S. A. Sabbagh, *Physical Review Letters* **105**, 135004 (2010).